Multi-Sonar Target Detection using Multi-Channel Coherence Analysis

Nick Klausner*, Mahmood R. Azimi-Sadjadi*, and J. Derek Tucker*†

*Department of Electrical and Computer Engineering
Colorado State University, Fort Collins, Colorado 80523-1373
Email: {nklausne,azimi,dtucker}@engr.colostate.edu

†Naval Surface Warfare Center - Panama City Division
Panama City, FL 32407-7001
Email: james.d.tucker@navy.mil

***Abstract*—The use of multiple disparate platforms in many remote sensing and surveillance applications allows one to exploit the coherent information shared among all sensory systems thereby potentially reducing the risk of making single-sensory biased detection and classification decisions. This paper introduces a target detection method based upon multi-channel coherence analysis (MCA) framework which optimally decomposes the multi-channel data to analyze their linear dependence or coherence. This decomposition then allows one to extract MCA features that can be used to implement a coherence-based detector. This detector is applied to a data set of underwater side-scan sonar imagery provided by the Naval Surface Warfare Center Panama City Division. This database contains data from 2 disparate sonar systems, namely one high frequency (HF) sonar and one broadband (BB) sonar coregistered over the same region on the sea floor. Test results illustrate the effectiveness of the proposed multi-platform detection system in terms of probability of detection, false alarm rate, and receiver operating characteristic (ROC) curves.**

***Index Terms*—Binary hypothesis testing, multiple disparate sonar systems, multi-channel coherence analysis, underwater target detection**

I. Introduction

The development of a robust underwater target detection and classification system that can operate with multiple disparate sensor systems and in different operating conditions poses many technical challenges. In the traditional centralized processing, preliminary detection, feature extraction and object classification are performed based upon the data collected using every sensor platform. A final decision-making usually takes place at the central station, either in the post-mission analysis (PMA) or real-time network-centric sensor analysis (NSA) modes, using some type of a decision, feature or combined fusion mechanism. However, decision-making based upon individual sensory data typically leads to incomplete, degraded or biased local (sensor-level) decisions hence resulting in an unacceptable final detection and classification performance at the fusion center.

In the collaborative decision-making using several sensor platforms, it is essential to detect and further scrutinize the information-bearing parts of the data collected by various platforms. This involves detecting, isolating and representing, in terms of some pertinent attributes, the *coherent* or common information among the multiple data sets. This is an extremely challenging problem due to the disparate nature of the problem and variations in the operating conditions. Thus, to develop a system-level solution, new methodologies are needed to: (a) collaboratively detect and agree on threats occurring within the field of view of the sensors, (b) perform collaborative feature extraction to capture common target attributes from multiple sensor platforms, (c) perform object classification and identification, (d) and finally develop a single integrated target assessment picture based upon the detected, localized and classified targets from multiple disparate sensors.

The existing work [1] - [2] in the area of target detection from sonar imagery has primarily been focused on one sonar platform, with fusion across multiple algorithms. In [3], the adaptive clutter filter detector in [2] is individually applied to three different sonar images varying in frequency and bandwidth. Final classification is done using an optimal set of features using a nonlinear log-likelihood ratio test where the decisions of the individual detector and classifier are fused. The optimal set of features is determined based upon cascading another classifier on the previous classifier during the training stage. This is done as a repeated application during the training stage where at each iteration the threshold and optimal feature set is chosen and updated. Canonical Correlation Analysis (CCA) [4], [5] was utilized in [6] to form a dual disparate detector in which detection decisions are based on the amount of coherent information shared among pairs of coregistered Regions of Interest (ROIs) from two different sonar images. This dual disparate detector is then applied to a distributed detection framework and is shown to exhibit high performance with a low false alarm rate and high probability of detection. MCA can be seen as a natural extension of CCA to more than two channels. In [7], MCA is applied to Landsat imagery to quantify the amount of coherent information from multiple spectral bands and across different images in time. In our previous work [8], [9], we developed a new framework for multi-sensor coherence analysis using MCA which can be

978-1-4244-4333-8/10/$25.00 ©2010 IEEE

applied to the data collected using multiple disparate sonar systems. In [8], this method was applied to a data set consisting of four disparate sonar images to study the performance of the detector to a varying number of channels. In [9], the method was then applied to a data set consisting of simulated target and non-target shapes embedded in simulated background to study the robustness of the detector to signal-to-noise ratio (SNR), target type, and aspect angle separation.

This paper reviews the N-channel coherence-based detector using the MCA framework [8]. This detector exploits the coherence of objects present in N disparate channels based on the assumption that the presence of objects in all data sets will lead to a higher level of coherence compared to that of noise alone. New expressions for the log-likelihood ratio and J-divergence in the MCA framework are provided and used for the simultaneous detection of targets from N disparate sonar data. The proposed detection framework is then implemented using a data set provided by the Naval Surface Warfare Center Panama City Division (NSWC PCD) that consists of one HF and one BB side-looking sonar imagery coregistered over the same region on the sea floor. This data set is substantially more challenging (due to dense background clutter) when compared with that of [8]. This would enable us to determine the real usefulness of this MCA-based detector.

This paper is organized as follows: Section II will review the MCA framework. Section III develops the MCA-based Gauss-Gauss detection method and presents new expressions for the log-likelihood ratio and J-divergence. Section IV provides the results of implementing the proposed detector on the NSWC PCD data set and finally concluding remarks will be made in Section V.

II. A Review of Multi-Channel Coherence Analysis

Consider N zero mean random vectors, $\mathbf{x}_1$, $\mathbf{x}_2$,..., and $\mathbf{x}_N$, representing multiple data channels comprising the composite data channel $\mathbf{z} = [\mathbf{x}_1^H \mathbf{x}_2^H ... \mathbf{x}_N^H]^H \in \mathbb{C}^{d\times 1}$. Without loss of generality, we will assume that all random vectors to be zero mean throughout this analysis. Let each channel $\mathbf{x}_j \in \mathbb{C}^{d_j \times 1}$ be of dimension d_j, where it is assumed that $\mathbf{x}_1$ is of the smallest dimension and we denote $d = \sum_{j=1}^{N} d_j$. The $d \times d$ dimensional covariance matrix of the composite data channel $\mathbf{z}$ is given by

$$R_{\mathbf{zz}} = E\left[\mathbf{z}\mathbf{z}^H\right] = \begin{bmatrix} R_{11} & R_{12} & \cdots & R_{1N} \\ R_{21} & R_{22} & \cdots & R_{2N} \\ \vdots & \vdots & \ddots & \vdots \\ R_{N1} & R_{N2} & \cdots & R_{NN} \end{bmatrix}, \quad (1)$$

where $R_{jk} = E[\mathbf{x}_j \mathbf{x}_k^H]$ is the auto-covariance ($j = k$) or cross-covariance ($j \neq k$) matrices of data channels $\mathbf{x}_j$ and $\mathbf{x}_k$ and clearly we have $R_{jk} = R_{kj}^H$.

Similar to CCA [10], [11] the i^{th} multi-channel coordinate of the j^{th} channel is found by searching for the i^{th} coordinate mapping vector, $\boldsymbol{\alpha}_{i,j}$, of data channel $\mathbf{x}_j$. This linear transformation produces the i^{th} multi-channel coordinate for the j^{th} channel,

$$v_{ij} = \boldsymbol{\alpha}_{i,j}^H \mathbf{x}_j. \quad (2)$$

If the i^{th} coordinate mapping vectors are found for all N channels, we can then obtain the *composite coordinate mapping* vector $\mathbf{a}_i = [\ \boldsymbol{\alpha}_{i,1}^H \ \ \boldsymbol{\alpha}_{i,2}^H \ \cdots \ \boldsymbol{\alpha}_{i,N}^H\ ]^H$. This is then used to find the *composite coordinate* vector $\mathbf{v}_i = [\ v_{i,1}^* \ \ v_{i,2}^* \ \cdots \ v_{i,N}^*\ ]^H = [\ \mathbf{x}_1^H \boldsymbol{\alpha}_{i,1} \ \ \mathbf{x}_2 \boldsymbol{\alpha}_{i,2} \ \cdots \ \mathbf{x}_N^H \boldsymbol{\alpha}_{i,N}\ ]^H$ which consists of the i^{th} multi-channel coordinate of every channel. Note that * denotes the complex conjugate operation. The associated covariance matrix of $\mathbf{v}_i$ is given by

$$R_{\mathbf{v}_i\mathbf{v}_i} = E\left[\mathbf{v}_i \mathbf{v}_i^H\right] = \begin{bmatrix} \boldsymbol{\alpha}_{i,1}^H R_{11} \boldsymbol{\alpha}_{i,1} & \cdots & \boldsymbol{\alpha}_{i,1}^H R_{1N} \boldsymbol{\alpha}_{i,N} \\ \vdots & \ddots & \vdots \\ \boldsymbol{\alpha}_{i,N}^H R_{N1} \boldsymbol{\alpha}_{i,1} & \cdots & \boldsymbol{\alpha}_{i,N}^H R_{NN} \boldsymbol{\alpha}_{i,N} \end{bmatrix}.$$

Recall that in the two-channel CCA [5], [12], the correlations between the mapped coordinates are maximized subject to the constraint that the transformed coordinates have unit variance. In the multi-channel case, however, the analysis is not as well-defined as all correlations between all possible pairs of channels must be maximized simultaneously. To accomplish this, one approach that has been offered [7] is to maximize the sum of all correlations (the SUMCOR objective function) subject to the unit trace constraint of matrix $R_{\mathbf{v}_i\mathbf{v}_i}$. Thus, the optimization problem for finding the first composite coordinate mapping vector $\mathbf{a}_1$ using the objective function and constraint just described becomes

$$\mathbf{a}_1 = \arg\max_{\mathbf{a}_1} \sum_{j=1}^{N}\sum_{k=1}^{N} \boldsymbol{\alpha}_{1,j}^H R_{j,k} \boldsymbol{\alpha}_{1,k} = \arg\max_{\mathbf{a}_1} \sum_{j=1}^{N}\sum_{k=1}^{N} [R_{\mathbf{v}_1\mathbf{v}_1}]_{j,k} \quad (3)$$

subject to the constraint

$$\mathrm{tr}\left(R_{\mathbf{v}_1\mathbf{v}_1}\right) = \sum_{j=1}^{N} \boldsymbol{\alpha}_{1,j}^H R_{jj} \boldsymbol{\alpha}_{1,j} = 1,$$

It is shown [7] that the constrained optimization problem for the first coordinate mapping vectors, $\boldsymbol{\alpha}_{1,j}$ using a Lagrange multiplier method leads to

$$\sum_{k=1}^{N} R_{jk} \boldsymbol{\alpha}_{1,k} = \lambda_1 R_{jj} \boldsymbol{\alpha}_{1,j}, \quad \forall \ \ j,k \in [1,N]$$

or in matrix notation as

$$R_{\mathbf{zz}} \mathbf{a}_1 = \lambda_1 D \mathbf{a}_1, \quad (4)$$

where D is a block diagonal matrix with diagonal blocks $R_{jj} \ \ \forall \ \ j \in [1,N]$, i.e.

$$D = \mathrm{diag}\left[R_{11}, R_{22}, \ldots, R_{NN}\right]. \quad (5)$$

The result in (4) represents a generalized eigenvalue problem for which standard methods of solution are well-known [13]. We will then consider the simultaneous solution to all mapping vectors $\mathbf{a}_i$'s, $i \in [1,d]$ and write (4) as $R_{\mathbf{zz}} A = DA\Lambda$ where A consists of all d coordinate mapping vectors, and Λ consists of all d eigenvalues. This solution can then be

rewritten in terms of a standard eigenvalue problem $EP = P\Lambda$ where $E = D^{-\frac{1}{2}} R_{\mathbf{zz}} D^{-\frac{H}{2}}$ and P is a unitary matrix $\left(PP^H = P^H P = I\right)$. Clearly, we can find the mapping matrix A via $A = D^{-\frac{H}{2}} P$.

Inspection of matrix E, which we refer to as the coherence matrix[1], shows that it is simply the composite covariance matrix of the whitened version of $\mathbf{z} = \left[\begin{array}{ccc} \mathbf{x}_1^H & \cdots & \mathbf{x}_N^H \end{array}\right]^H$. That is, if we define this whitened version of the composite data channel vector by $\mathbf{w} = \left[\begin{array}{ccc} \mathbf{w}_1^H & \cdots & \mathbf{w}_N^H \end{array}\right]^H = D^{-\frac{1}{2}}\mathbf{z}$, then the whitened composite vector $\mathbf{w}$ has correlation matrix $E\left[\mathbf{w}\mathbf{w}^H\right] = D^{-\frac{1}{2}} R_{\mathbf{zz}} D^{-\frac{H}{2}} = E$. Matrix P is then used to map the whitened channels to their multi-channel coordinates. In order to find mapping vectors corresponding to the principal coordinates [7], we only consider the $r = d_1 = \min_j \{d_j\}$ coordinates such that $\lambda_1 > \lambda_2 > \ldots > \lambda_r$. Thus, $\Lambda = \text{diag}\left[\lambda_1, \lambda_2, \ldots, \lambda_r\right]$ will become a $r \times r$ diagonal matrix composed of the dominant eigenvalues and P will become a $d \times r$ matrix composed of the eigenvectors corresponding to r dominant eigenvalues.

To find the mapped coordinate vector, $\mathbf{v}$, that contains all mapped coordinates for all N channels, we will first define Ψ_j (dimension $d_j \times r$) to contain those dominant r eigenvectors $\mathbf{p}_{i,j}, \forall \;\; i \in [1, r]$ of the mapping matrix P that correspond to the j^{th} channel

$$\Psi_j = \left[\begin{array}{cccc} \mathbf{p}_{1,j} & \mathbf{p}_{2,j} & \cdots & \mathbf{p}_{r,j} \end{array}\right], \; \forall \; j \in [1, N]. \quad (6)$$

Clearly, the connection between P and Ψ_j is evident

$$P = \left[\begin{array}{c} \Psi_1 \\ \Psi_2 \\ \vdots \\ \Psi_N \end{array}\right]_{d \times r}. \quad (7)$$

Note that in the case of two channels, Ψ_1 and Ψ_2 become the mapping matrices of CCA [4]. All of the mapped coordinates of the j^{th} channel can then be found by

$$\boldsymbol{\mu}_j = \Psi_j^H R_{jj}^{-\frac{1}{2}} \mathbf{x}_j, \quad \forall \;\; j \in [1, N], \quad (8)$$

where $\boldsymbol{\mu}_j = \left[\begin{array}{cccc} v_{1,j}^* & v_{2,j}^* & \cdots & v_{r,j}^* \end{array}\right]^H$. Clearly, we have the following two properties

$$\begin{aligned} \sum_{j=1}^{N} E\left[\boldsymbol{\mu}_j \boldsymbol{\mu}_j^H\right] &= \sum_{j=1}^{N} \Psi_j^H \Psi_j = I \\ \sum_{j=1}^{N}\sum_{k=1}^{N} E\left[\boldsymbol{\mu}_j \boldsymbol{\mu}_k^H\right] &= \sum_{j=1}^{N}\sum_{k=1}^{N} \Psi_j^H R_{jj}^{-\frac{1}{2}} R_{jk} R_{kk}^{-\frac{H}{2}} \Psi_k = \Lambda \end{aligned}$$

If we define block diagonal matrix $\boldsymbol{\Psi}$ that contains the Ψ_j matrices along its diagonal blocks, i.e. $\boldsymbol{\Psi} = \text{diag}\left[\Psi_1, \Psi_2, \ldots, \Psi_N\right]$, then we can resolve all N channels into their multi-channel coordinates using

$$\mathbf{v} = \boldsymbol{\Psi}^H \mathbf{w} = \boldsymbol{\Psi}^H D^{-\frac{1}{2}} \mathbf{z}. \quad (9)$$

Figure 1 displays the process behind the MCA analysis filter.

[1]Note that in the two-channel CCA, the off-diagonal blocks of this matrix relate to the coherence matrix [5]

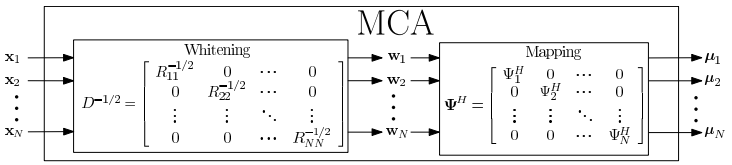

Fig. 1: MCA Processing Block Diagram.

As can be seen, similar to CCA [5] all channels are whitened in order to remove the auto-correlation contributions from each individual component thereby allowing one to analyze the linear dependence shared among one another using matrix $\boldsymbol{\Psi}$.

III. MCA Detection

A classical detection problem is that of choosing between two hypotheses that are relevant to the given problem. For this coherence-based detector, the null hypothesis (H_0) is the hypothesis that all N MCA channels consist of background noise and the alternative hypothesis (H_1) that all N MCA channels consist of signal plus noise. Figure 2 shows the graphical setup of the problem under consideration. Several simplifying but sensible assumptions used in this analysis are

1) Noise between different channels is mutually uncorrelated, i.e. $E\left[\mathbf{n}_j \mathbf{n}_k^H\right] = 0 \; \forall \; j, k \in [1, N], \; j \neq k$.
2) Signal is uncorrelated with the background noise, i.e. $E\left[\mathbf{s}_j \mathbf{n}_k^H\right] = E\left[\mathbf{n}_j \mathbf{s}_k^H\right] = 0 \; \forall \; j, k \in [1, N]$.
3) Noise contained on any one channel has covariance matrix, i.e. $E\left[\mathbf{n}_j \mathbf{n}_j^H\right] = R_{\mathbf{n}_j} \; \forall \; j \in [1, N]$.
4) Signal contained on any pair of channels has covariance matrix, i.e. $E\left[\mathbf{s}_j \mathbf{s}_k^H\right] = R_{\mathbf{s}_{jk}} \; \forall \; j, k \in [1, N]$.

Under H_0, the matrices $R_{\mathbf{zz}}$ and D become

$$R_{\mathbf{zz}_0} = D_0 = \text{diag}\left[R_{\mathbf{n}_1}, R_{\mathbf{n}_2}, \ldots, R_{\mathbf{n}_N}\right].$$

Note that the subscript notation refers to the hypothesis being considered.

Under H_1 and using the stated assumptions, the corresponding $R_{\mathbf{zz}}$ and D matrices are

$$\begin{aligned} R_{\mathbf{zz}_1} &= \left[\begin{array}{cccc} R_{\mathbf{s}_{11}} + R_{\mathbf{n}_1} & R_{\mathbf{s}_{12}} & \cdots & R_{\mathbf{s}_{1N}} \\ R_{\mathbf{s}_{21}} & R_{\mathbf{s}_{22}} + R_{\mathbf{n}_2} & \cdots & R_{\mathbf{s}_{2N}} \\ \vdots & \vdots & \ddots & \vdots \\ R_{\mathbf{s}_{N1}} & R_{\mathbf{s}_{N2}} & \cdots & R_{\mathbf{s}_{NN}} + R_{\mathbf{n}_N} \end{array}\right] \\ D_1 &= \text{diag}\left[R_{\mathbf{s}_{11}} + R_{\mathbf{n}_1}, R_{\mathbf{s}_{22}} + R_{\mathbf{n}_2}, \ldots, R_{\mathbf{s}_{NN}} + R_{\mathbf{n}_N}\right] \end{aligned}$$

leading to the following arbitrary eigenvalue problem.

$$R_{\mathbf{zz}_1} A_1 = D_1 A_1 \Lambda_1 \quad (10)$$

The log-likelihood ratio that minimizes the risk involved in deciding between the two hypotheses is defined [5], [12] to be

$$l(\mathbf{z}) = \ln\left[\frac{p(\mathbf{z}|H_1)}{p(\mathbf{z}|H_0)}\right] \quad (11)$$

Assuming that under both hypotheses the composite data channel $\mathbf{z}$ is multivariate Gaussian with zero mean and covariance

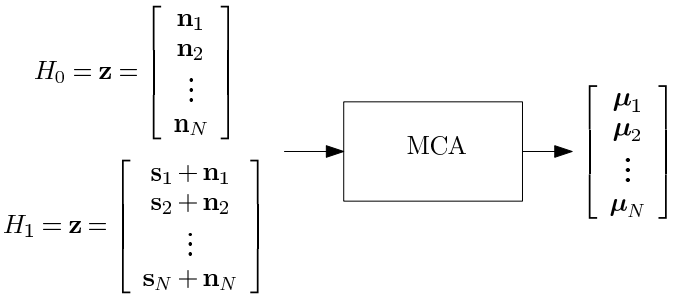

Fig. 2: Multi-Channel Hypothesis Test and MCA.

matrix $R_{\mathbf{zz}}$, the log-likelihood ratio of the composite data vector becomes

$$l(\mathbf{z}) = \mathbf{z}^H \left(R_{\mathbf{zz}_0}^{-1} - R_{\mathbf{zz}_1}^{-1} \right) \mathbf{z}. \tag{12}$$

Next, we can formulate $R_{\mathbf{zz}}^{-1}$ in terms of the sum of the correlations of each coordinate and their corresponding eigenvectors. To do this, we recall the fact that $P^H E P = \Lambda$. Taking the inverse of this relationship, it is simple to show that $R_{\mathbf{zz}}^{-1} = D^{-H/2} P \Lambda P^H D^{-1/2}$. Thus, the log-likelihood function of (12) becomes

$$l(\mathbf{z}) = \mathbf{z}^H \left(D_0^{-1} - D_1^{-H/2} P_1 \Lambda_1^{-1} P_1^H D_1^{-1/2} \right) \mathbf{z}.$$

We then remove the second-order information associated with the H_1 hypothesis from each individual channel by "whitening" with the filter $D_1^{-1/2}$ so that

$$\begin{aligned} \mathbf{z} &\rightarrow \mathbf{w} = D_1^{-1/2} \mathbf{z} \\ E_{H_0}\left[\mathbf{w}\mathbf{w}^H\right] &= D_1^{-1/2} D_0 D_1^{-H/2} = \Sigma^{-1} \\ E_{H_1}\left[\mathbf{w}\mathbf{w}^H\right] &= D_1^{-1/2} R_{\mathbf{zz}_1} D_1^{-H/2} = P_1 \Lambda_1 P_1^H \end{aligned}$$

where the matrix Σ is in some sense a *local* SNR matrix with the j^{th} diagonal block equal to

$$\Sigma_j = \left(R_{\mathbf{s}_{jj}} + R_{\mathbf{n}_j} \right)^{H/2} R_{\mathbf{n}_j}^{-1} \left(R_{\mathbf{s}_{jj}} + R_{\mathbf{n}_j} \right)^{1/2}$$

The log-likelihood ratio in this new coordinate system then becomes

$$l(\mathbf{z}) = \mathbf{w}^H \left(\Sigma - P_1 \Lambda_1^{-1} P_1^H \right) \mathbf{w}$$

Finally, we map our data into the MCA coordinate system (under H_1) through the filter P_1 so that

$$\begin{aligned} \mathbf{w} &\rightarrow \bar{\mathbf{v}} = P_1^H \mathbf{w} \\ E_{H_0}\left[\bar{\mathbf{v}}\bar{\mathbf{v}}^H\right] &= P_1^H \Sigma^{-1} P_1 \\ E_{H_1}\left[\bar{\mathbf{v}}\bar{\mathbf{v}}^H\right] &= \Lambda_1 \end{aligned}$$

where Λ_1 is a matrix with the sum of the correlations of the MCA coordinates under H_1 along its diagonal. We can then rewrite the log-likelihood ratio as

$$l(\mathbf{z}) = \bar{\mathbf{v}}^H \left(P_1^H \Sigma P_1 - \Lambda_1^{-1} \right) \bar{\mathbf{v}} \tag{13}$$

where $\bar{\mathbf{v}} = \left[\sum_{j=1}^N v_{1,j} \ \cdots \ \sum_{j=1}^N v_{d,j} \right]^T$ is a vector of the sum of the MCA coordinates under H_1. Again, this is still the standard Gauss-Gauss log-likelihood ratio presented in [12], but in the coordinates $P_1^H D_1^{-1/2} \mathbf{z}$. However, the detector built here searches for coherence structure among all pairwise combinations of channels under H_1. MCA is then used to "discover" the coherence structure among the channels by solving a generalized eigenvalue problem. The amount of coherence in each MCA coordinate can then be interpreted and analyzed through the generalized eigenvalue, λ_i.

Next, we will formulate the J-divergence [12], [14] which is a measure of the separability of the two hypotheses. The J-divergence is defined to be

$$J = E_{H_1}\left[l(\mathbf{z}) \right] - E_{H_0}\left[l(\mathbf{z}) \right], \tag{14}$$

where $E_{H_1}[\,\cdot\,]$ and $E_{H_0}[\,\cdot\,]$ represent the expectation operation evaluated under the H_1 and H_0 hypotheses, respectively. The expected value of the log-likelihood function becomes

$$E\left[l(\mathbf{z}) \right] = E\left[tr\left(\mathbf{z}^H Q \mathbf{z} \right) \right] \tag{15}$$

where $Q = \left(R_{\mathbf{zz}_0}^{-1} - R_{\mathbf{zz}_1}^{-1} \right)$. Using the cyclic property of the trace, we can write

$$\begin{aligned} E\left[l(\mathbf{z}) \right] &= E\left[tr\left(Q \mathbf{z}\mathbf{z}^H \right) \right] \\ &= tr\left(Q R_{\mathbf{zz}} \right). \end{aligned} \tag{16}$$

Thus, we can write the J-divergence as

$$\begin{aligned} J &= E_{H_1}\left[l(\mathbf{z}) \right] - E_{H_0}\left[l(\mathbf{z}) \right] \\ &= tr\left(Q R_{\mathbf{zz}_1} \right) - tr\left(Q R_{\mathbf{zz}_0} \right) \\ &= tr\left[-2I + R_{\mathbf{zz}_0}^{-1} R_{\mathbf{zz}_1} + R_{\mathbf{zz}_1}^{-1} R_{\mathbf{zz}_0} \right]. \end{aligned} \tag{17}$$

Rearranging and using the cyclic property of the trace, we can write the J-divergence as

$$J = \text{tr}\left(-2I + \Lambda_1 P_1^H \Sigma P_1 + \Lambda_1^{-1} P_1^H \Sigma^{-1} P_1 \right) \tag{18}$$

$$= \sum_{i=1}^{d} \left(-2 + \mathbf{p}_i^H \left[\lambda_i \Sigma + (\lambda_i \Sigma)^{-1} \right] \mathbf{p}_i \right). \tag{19}$$

Therefore, we find that the divergence in the MCA coordinate system becomes decomposed in terms of the MCA generalized eigenvalue, λ_i, and also the two quadratic terms, $\mathbf{p}_i^H \Sigma \mathbf{p}_i$ and $\mathbf{p}_i^H \Sigma^{-1} \mathbf{p}_i$. The quadratic term $\mathbf{p}_i^H \Sigma \mathbf{p}_i$ in some sense gives us a scalar measurement of the sum of the local signal-to-noise ratios in the one-dimensional subspace spanned by $\mathbf{p}_i$. Thus, it appears that writing the J-divergence in this manner decomposes the information needed for detection into the coherence shared between data channels (λ_i) and the coherent information among the individual channels themselves ($\mathbf{p}_i^H \Sigma \mathbf{p}_i$).

Because of the structure of target and background data in sonar imagery, it can be justifiable to assume that the local signal-to-noise ratios of each channel are very small but the coherence shared between pairs of channels is significant for detection and approximate the matrix Σ with the identity matrix ($\Sigma \approx I$). Such a situation arises when the distribution of the data associated with any particular channel is similar under both H_0 and H_1 and yet there exists a sufficient amount of cross-correlation between data channels under H_1

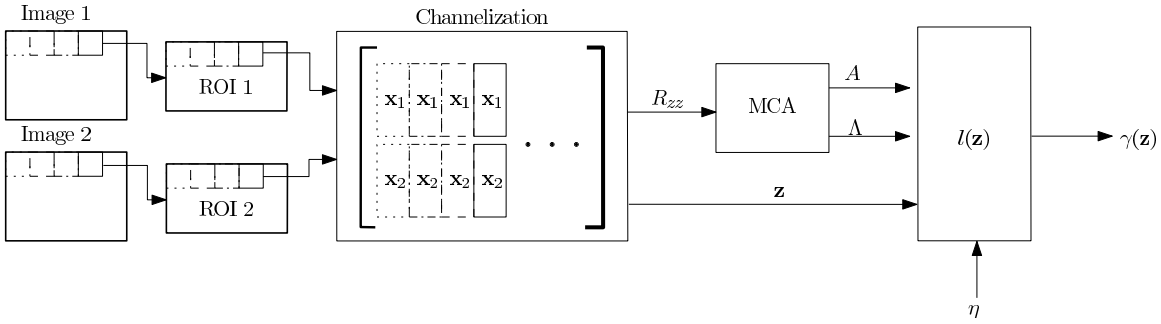

Fig. 3: Dual Channel Detection System

to perform detection. In such cases, the log-likelihood ratio can be approximated by the equation

$$l(\mathbf{z}) \approx \bar{\mathbf{v}}^H \left(I - \Lambda^{-1}\right) \bar{\mathbf{v}} \tag{20}$$

with an associated J-divergence

$$J \approx \sum_{i=1}^{d} \left(-2 + \lambda_i + \lambda_i^{-1}\right) \tag{21}$$

Therefore, in such a situation we disregard the coherent information among each individual channel and focus our attention around detecting the presence of coherence among the data channels.

IV. Multi-Platform Test Results

The MCA-based coherence detector is applied to a dual-sonar data set consisting of one HF high-resolution side-scan sonar image as well as one BB sonar image. For a review of HF and BB sonar systems, the reader is referred to [15] and [16]. As mentioned previously, multiple sonar detection is favorable over single sonar detection as the detector has multiple independent looks at the same target thereby increasing the wealth of information available for the detection decisions. Because a HF sonar provides higher spatial resolution and better ability to capture target details and characteristics while a BB sonar offers much better clutter suppression ability with lower spatial resolution, performing detection with combinations of multiple HF and BB images can also be advantageous.

The image database used in this study contains over 1200 pairs of HF and BB co-registered sonar images containing 99 objects of interest with some images containing more than one object of interest. Objects of interest are then further categorized into 49 target objects and 50 lobster trap objects. When implementing the MCA-based detection system, each pair of images is partitioned, with 50% overlap in both the range and cross-range dimensions, into ROIs of size 72×112 and 24×224 for the HF and BB sonar images, respectively. Each ROI is then partitioned with a rectangular blocking scheme with no overlap using block sizes of 6×4 and 2×8 for the HF and BB ROIs, respectively. Each pair of blocks is then channelized to form the composite observation $\mathbf{z}$. All HF and BB blocks pertaining that pair of co-registered ROIs then form an ensemble set from which the sample composite covariance matrix $R_{\mathbf{zz}}$ is computed. Using this matrix, the correlation and MCA mapping matrices are extracted and used to form the log-likelihood function given in (20). Each composite realization from the ensemble set corresponding to that pair of ROIs is then applied to the log-likelihood ratio test and compared to a threshold designated by the user. If 50% or more pass, a call to the H_1 hypothesis is made. Figure 3 displays the process behind this dual sonar detection system.

From the entire dual-sonar data set, a partial subset of images containing 50 objects of interest (25 targets, 25 lobster traps) is extracted. This is done to observe the response of the detection system to a threshold that is determined and tested on two independent data sets. Using the 50 objects of interest and a same size set of background ROIs, an optimal threshold of 0.5212 was experimentally chosen.

To study the separability of the principal multi-channel correlations between ROIs that contain objects of interest immersed in background and those that solely contain background, a test was conducted on the entire target and lobster trap set ROIs corresponding to all 99 objects of interest and a same size randomly selected set of ROIs containing only background clutter. Figures 4(a) and (b) exhibit plots of the mean and standard deviation for each of the dominant 16 multi-channel correlations for targets and lobster traps as well as background clutter for this data set. As can be seen in Figure 4(a), there is suitable separation among the principal MCA correlations pertaining to objects of interest versus those pertaining to background alone. We can also see a noticeable difference (see Figure 4(b)) among the statistics of the MCA correlations pertaining to targets and lobster traps as the separation among target and non-target features seems to be larger than that among lobster trap and non-target features. These figures suggest that the MCA correlations may provide a useful set of features for discriminating among target and target-like objects when applied to a classifier. However, this is merely an observation and will not be discussed further in this paper.

The dual-sonar detection system is then implemented on the test set containing 49 objects of interest (24 targets, 25 lobster traps) using the predetermined threshold mentioned above. A histogram of the likelihood values for an example target ROI as well as an ROI containing background clutter

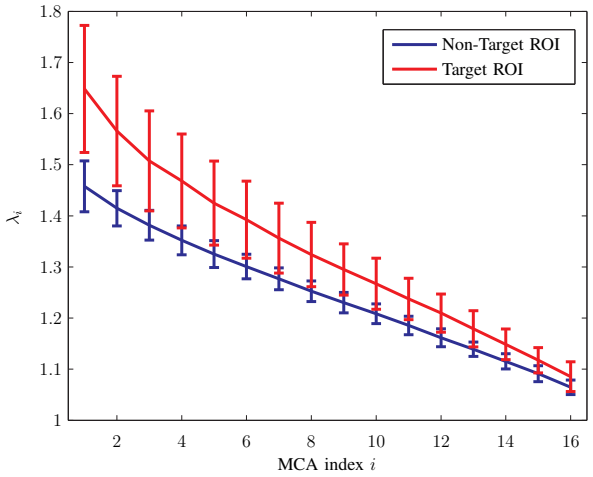

(a) Target and Background

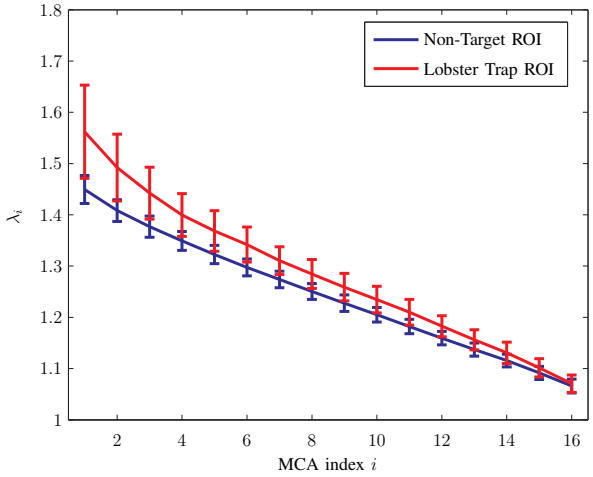

(b) Lobster Trap and Background

Fig. 4: Plot of Multi-Channel Correlations for Target, Lobster Trap, and Background ROIs.

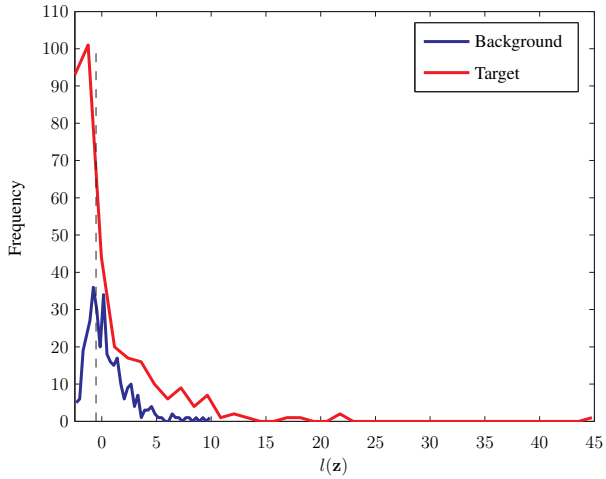

Fig. 5: Histogram of Likelihood Values for Target and Non-Target ROIs

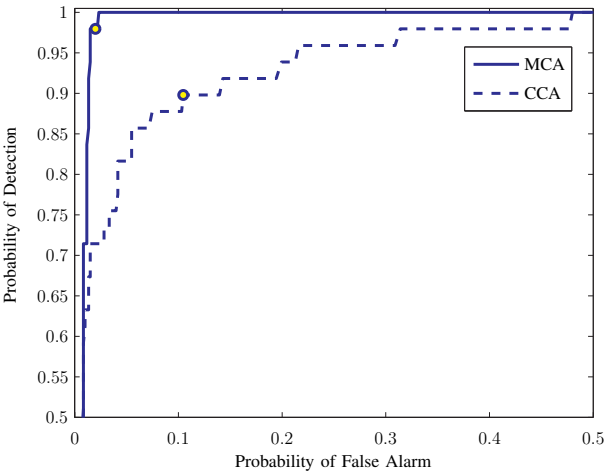

Fig. 6: Receiver-Operator Characteristics Curve

is shown in Figure 5. The threshold of 0.5212 determined previously is shown as a dotted line. As we can see from the figure, there is a suitable amount of distinction among target and background likelihood values exhibiting high detectability. This dual-sonar detection system detects all 49 objects with an average of 7 false alarms per image which is an excellent detection performance given the challenging nature of this data set. The ROC curve for the detection system applied to the subset of images containing 49 objects of interest is displayed in Figure 6. The detector exhibits $P_d = 98\%$ and $P_{fa} = 2\%$ at the knee-point of the ROC curve (where $P_d + P_{fa} = 1$) which is associated with a threshold of 0.6525. This threshold corresponding to the knee-point of the ROC curve is nearly equal to the predetermined threshold of 0.5212 used for the test suggesting a low sensitivity to novel data. A knee-point probability of detection of 98% corresponds to one missed object which in this case was a lobster trap. Also shown in Figure 6 is the ROC curve associated with the dual disparate detector in [6] based on two-channel CCA. This detection method exhibits $P_d = 90\%$ and $P_{fa} = 10\%$ at the knee point of the ROC curve for the same data set consisting of 49 objects of interest. The stark contrast in performance among the two methods may possibly be attributed to the simplistic assumptions made in developing the method presented in [6]. Overall, we can see that the detection system tested performs very well with a high probability of detection and low false alarm rate even though a small number of targets and non-targets were used to form the detection threshold.

V. Conclusion

A new multi-channel, multi-sonar binary hypothesis detection system has been introduced using the MCA framework. An N-channel Gauss-Gauss detector is then formulated in the MCA coordinates. Detection is performed by extracting

the multi-channel mapping vectors and the correlation sums from the data samples collected by the sonar systems. These mapping vectors and coherent features are then used in the log-likelihood ratio to detect targets in the dual sonar images. This MCA-based detector is then applied to a dual-sonar data set consisting of one HF sonar and one BB sonar with disparateness in frequency and resolution. The statistics of MCA correlations are found to exhibit separation among target and target-like objects suggesting the possibility of using these features for the purposes of target vs. non-target classification. A threshold is determined from a partial subset of images and the MCA-based detection system is then tested on the remaining images. The detector performed exceptionally well with a probability of detection at 100% while maintaining 7 false alarms per image. Through this work we have shown that MCA provides a robust and elegant framework when performing coherence-based detection among multiple disparate sensory channels.

ACKNOWLEDGMENT

This work was supported by the Office of Naval Research, Code 321OE under contract #N00014-08-1-0142.

REFERENCES

[1] G. J. Dobeck, J. Hyland, and L. Smedley, "Automated detection/classification of sea mines in sonar imagery," *Proc. SPIE*, vol. 3079, pp. 90–110, April 1997.

[2] T. Aridgides, P. Libera, M. Fernandez, and G. J. Dobeck, "Adaptive filter/feature orthogonalization processing string for optimal LLRT mine classification in side-scan sonar imagery," *Proc. SPIE*, vol. 2765, pp. 110–121, April 1996.

[3] T. Aridgides and M. Fernandez, "Enhanced ATR algorithm for high resolution multi-band sonar imagery," *Proc. SPIE*, vol. 6953, pp. 0H1–0H10, March 2008.

[4] L. Scharf and C. Mullis, "Canonical coordinates and the geometry of inference, rate, and capacity," *IEEE Transactions on Signal Processing*, vol. 48, pp. 824–831, March 2000.

[5] A. Pezeshki, L. Scharf, J. Thomas, and B. Van Veen, "Canonical coordinates are the right coordinates for low-rank Gauss-Gauss detection and estimation," *IEEE Transactions on Signal Processing*, vol. 54, pp. 4817–4820, December 2006.

[6] J. D. Tucker, N. Klausner, and M. R. Azimi-Sadjadi, "Target detection in m-disparate sonar platforms using multichannel hypothesis testing," *Proc. of MTS/IEEE Oceans 2008 Conference*, pp. 1–7, Sep. 2008.

[7] A. Neilsen, "Multiset canonical correlations analysis and multispectral, truly multitemporal remote sensing data," *IEEE Transactions on Image Processing*, vol. 11, pp. 293–305, March 2002.

[8] N. Klausner, M. R. Azimi-Sadjadi, and J. D. Tucker, "Underwater target detection from multi-platform sonar imagery using multi-channel coherence analysis," *Proc. of IEEE SMC 2009 Conference*, pp. 2728–2733, 2009.

[9] N. Klausner, J. D. Tucker, and M. R. Azimi-Sadjadi, "Multi-platform target detection using multi-channel coherence analysis and robustness to the effects of disparity," *Proc. of MTS/IEEE Oceans 2009 Conference*, pp. 1–7, October 2009.

[10] H. Hotelling, "Relations between two sets of variates," *Biometrika*, vol. 28, pp. 321–377, 1936.

[11] A. Rencher, *Methods of Multivariate Analysis*, 2nd ed. Wiley-Interscience, 2002.

[12] L. Scharf and B. Van Veen, "Low rank detectors for Gaussian random vectors," *IEEE Transactions on Acoustics, Speech, and Signal Processing*, vol. 35, pp. 1579–1582, November 1987.

[13] G. H. Golub and C. F. V. Loan, *Matrix Computations*, 3rd ed. John Hopkins University Press, 1996.

[14] S. Kullaback, *Information Theory and Statistics*. New York: Dover, 1968.

[15] W. Key, "Side scan sonar technology," *Proc. Oceans'00*, vol. 2, pp. 1029–1033, Sept 2000.

[16] S. Butler, "Triply resonant broadband transducers," *Oceans '02 MTS/IEEE*, vol. 4, pp. 2334–2341 vol.4, 29-31 Oct. 2002.